Celestial Mechanics and Dynamical Astronomy manuscript No.
(will be inserted by the editor)

G. Mingotti · F. Topputo · F. Bernelli-Zazzera

Low-Energy, Low-Thrust Transfers to the Moon

Received: date / Accepted: date

Abstract The low-thrust version of the low energy transfers to the Moon exploiting the structure of the invariant manifolds associated to the Lagrange point orbits is presented in this paper. A method to systematically produce low-energy, low-thrust transfers executing ballistic lunar capture is discussed. The coupled restricted three-body problems approximation is used to deliver appropriate first guess for the subsequent optimization of the transfer trajectory within a complete four-body model using direct transcription and multiple shooting strategy. It is shown that less propellant than standard low energy transfers to the Moon is required. This paper follows previous works by the same authors aimed at integrating together knowledge coming from dynamical system theory and optimal control problems for the design of efficient low-energy, low-thrust transfers.

Keywords Low Energy Transfer · Low-Thrust Transfer · Ballistic Capture · Lagrange Points · Invariant Manifolds · Three-Body Problem

1 Introduction

Low energy transfers to the Moon are being studied since the rescue of the Japanese spacecraft Hiten in 1991 [1]. In essence, a low energy lunar transfer reduces the hyperbolic excess velocity upon Moon arrival, typical of a patched-conics approach. This process is called ballistic capture, and relies on a better exploitation of the gravitational nature ruling the transfer problem instead of the classic Keplerian decomposition of the solar system. The reduced speed relative to the Moon sets the trajectory to low energy levels which in turn imply a reduced propellant mass needed to stabilize the spacecraft around the Moon.

It is known that the dynamical mechanism governing a class of exterior low energy transfers to the Moon is related to the structure of the invariant manifolds associated to the Lyapunov orbits about the collinear Lagrange points [2]. In particular, a systematic method for the construction of low energy transfers using the knowledge of the phase space of the Sun–Earth and Earth–Moon systems is given in [3]. With the "coupled restricted three-body problems approximation",

Giorgio Mingotti, Francesco Topputo, and Franco Bernelli-Zazzera
Politecnico di Milano, Dipartimento di Ingegneria Aerospaziale
Via La Masa, 34 – 20156, Milano, Italy
Tel.: +39-02-2399-8310/8640/8328; Fax: +39-02-2399-8334
E-mail: {giorgio.mingotti, francesco.topputo, franco.bernelli}@polimi.it

the four-body dynamics, characterizing the low energy lunar transfers, is decomposed into two restricted three-body problems, and the invariant manifolds of the Lyapunov orbits are computed. It is possible to show that, with a suitably chosen Poincaré section, the trajectory design is restricted to the selection of a single point on this section [3]. Flown backward, this initial condition gives rise to a trajectory close to the stable and unstable manifolds of the $L_{1,2}$ Lyapunov orbits of the Sun–Earth system; integrated forward, a transit, lunar ballistic capture orbit (i.e., an orbit contained inside the stable manifold of the L_2 Lyapunov orbit of the Earth–Moon system) is achieved. A small Δv maneuver is eventually needed at this patching point in order to match the energies of the two legs. With this approach it is possible to find efficient Earth–Moon transfers like the ones described in [1].

In the present work the low-thrust version of the transfers described in [3] is presented. It is in fact possible to further reduce the propellant necessary to send a spacecraft to the Moon by exploiting both the simultaneous gravitational attractions of the Sun, the Earth, and the Moon, and the high specific impulse provided by the low-thrust engines (e.g., ion engines). Nevertheless, including the low-thrust is not trivial, and asks for a number of issues that have to be dealt with. It is of great importance, for instance, overcoming the loss of Jacobi integral, finding subsets of the phase space that lead to low-thrust ballistic capture (playing the separatrix-like role of the stable manifold associated to L_2 Lyapunov orbit of the Earth–Moon system), and summarizing, using as few parameters as possible, all the reachable orbits that is possible to target with the finite thrust magnitude available. The purposes of this paper are therefore:

(i) to understand how the incorporation of low-thrust propulsion modifies the methodology described in [3];
(ii) to formulate a systematic method for the design of low-energy, low-thrust Earth-to-Moon transfers;
(iii) to demonstrate that a combined low-energy, low-thrust approach gives rise to transfers that both require even less propellant than the standard low energy transfers and still exploit the structure of the phase space of the two restricted-three body problems.

It is worth mentioning that previous works have faced the combination of n-body dynamics with low-thrust propulsion. An interior ballistic capture state using low-thrust propulsion was found in [4]. This approach paved the way for the design of the trajectory for ESA's SMART-1 mission [5]. Earth–Venus transfers have been obtained in [6] by combining invariant manifold dynamics and low-thrust with set oriented methods. A previous work by the present authors was devoted to the integration of dynamical system theory and optimal control problems for the design of efficient low-energy, low-thrust transfers to the halo orbits [7].

The remainder of the paper is organized as follows. In Section 2 the equations of the controlled restricted three-body and four-body problems are given, and the basic properties of these two models are recalled. In Section 3 we describe the design strategy that is used to find first guess solutions that are later optimized with the method discussed in Section 4. Low energy low-thrust transfers are presented in Section 5 and compared to reference works. Final considerations are made in Section 6.

2 Dynamical Models

The controlled motion of a spacecraft under the influence of two and three primaries is described in this section using the planar circular restricted three-body problem and the bicircular four-body problem, RTBP and RFBP, respectively, from now on.

2.1 Controlled Planar Restricted Three-Body Problem

The motion of the spacecraft, P_3, is studied in the gravitational field generated by the mutual circular motion of two primaries, P_1, P_2 of masses m_1, m_2, respectively, about their common center of mass. It is assumed that P_3 moves in the same plane of P_1, P_2 under the equations [8]

$$\ddot{x} - 2\dot{y} = \frac{\partial \Omega_3}{\partial x}, \qquad \ddot{y} + 2\dot{x} = \frac{\partial \Omega_3}{\partial y}, \tag{1}$$

where

$$\Omega_3(x, y, \mu) = \frac{1}{2}(x^2 + y^2) + \frac{1-\mu}{r_1} + \frac{\mu}{r_2} + \frac{1}{2}\mu(1-\mu), \tag{2}$$

and $\mu = m_2/(m_1 + m_2)$ is the mass parameter of the three-body problem. Equations (1) are written in barycentric rotating frame with nondimensional units: the angular velocity of P_1, P_2, their distance, and the sum of their masses are all set to 1. It is easy to verify that P_1, of mass $1-\mu$, is located at $(-\mu, 0)$, whereas P_2, of mass μ, is located at $(1-\mu, 0)$; thus, the distances between P_3 and the primaries are

$$r_1^2 = (x+\mu)^2 + y^2, \qquad r_2^2 = (x+\mu-1)^2 + y^2. \tag{3}$$

For fixed μ, the Jacobi integral reads

$$J(x, y, \dot{x}, \dot{y}) = 2\Omega_3(x, y) - (\dot{x}^2 + \dot{y}^2), \tag{4}$$

and, for a given energy C, it defines a three-dimensional manifold

$$\mathcal{J}(C) = \{(x, y, \dot{x}, \dot{y}) \in \mathbb{R}^4 | J(x, y, \dot{x}, \dot{y}) - C = 0\}, \tag{5}$$

foliating the four-dimensional phase space. The projection of $\mathcal{J}(C)$ on the configuration space (x, y) defines the Hill's curves bounding the allowed and forbidden regions associated to prescribed values of C. The vector field defined by (1) has five well-known equilibrium points, known as the Lagrange points, labeled L_k, $k = 1, \ldots, 5$. This study deals with the portion of the phase space surrounding the two collinear points L_1 and L_2. In a linear analysis, these two points behave like the product saddle $\times$ center. Thus, there exists a family of retrograde Lyapunov orbits and two-dimensional stable and unstable manifolds emanating from them [9, 10].

Equations (1) describe the ballistic motion of P_3. To model the *controlled* motion of P_3 under both the gravitational attractions of P_1, P_2, and the low-thrust propulsion, the following differential equations are considered

$$\ddot{x} - 2\dot{y} = \frac{\partial \Omega_3}{\partial x} + \frac{T_x}{m}, \qquad \ddot{y} + 2\dot{x} = \frac{\partial \Omega_3}{\partial y} + \frac{T_y}{m}, \qquad \dot{m} = -\frac{T}{I_{sp}\, g_0}, \tag{6}$$

where $T = \sqrt{T_x^2 + T_y^2}$ is the thrust magnitude, whereas I_{sp} and g_0 are, respectively, the specific impulse of the engine and the gravitational acceleration at sea level. Following observations arise by comparing systems of Equations (1) to (6):

- the ballistic motion is represented by a fourth-order system, while the controlled motion is described by a fifth-order system of differential equations. Variations of the spacecraft mass, m, are taken into account;
- the thrust in Equations (6) is not given, but rather in our approach it represents an unknown of the optimal control problem. It is determined such that a certain state is targeted and, at the same time, a certain objective function is minimized — this is a considerable difference between the present work and [6];

- in addition to the well-known cases where P_3 impacts with P_1 and P_2, the vector field of the controlled Equations (6) exhibits another singularity that is found when $m \to 0$. Special attention has to be paid to the thrust profile in the optimization phase to avoid this singularity.

Equations (6) are used to initially decompose the RFBP into two RTBP: the pair $\{P_1,\ P_2\}$ is represented by {Sun, Earth} in the first one, and by {Earth, Moon} in the second one, respectively. For brevity sake we refer to SE and EM models. The mass parameters assumed for these models are $\mu_{SE} = 3.0359\,10^{-6}$ and $\mu_{EM} = 1.2150\,10^{-2}$, respectively.

2.2 Controlled Planar Restricted Four-Body Problem

In the second part of the paper, solutions obtained with the coupled RTBP approximation are optimized within a four-body model. In principle, this system incorporates the perturbation of the Sun into the EM model. The equations of motion are

$$\ddot{x} - 2\dot{y} = \frac{\partial \Omega_4}{\partial x} + \frac{T_x}{m}, \quad \ddot{y} + 2\dot{x} = \frac{\partial \Omega_4}{\partial y} + \frac{T_y}{m}, \quad \dot{\theta} = \omega_S, \quad \dot{m} = -\frac{T}{I_{sp}\, g_0}, \tag{7}$$

where this time the potential Ω_4 is

$$\Omega_4(x, y) = \Omega_3(x, y, \mu_{EM}) + \frac{m_s}{r_s} - \frac{m_s}{\rho^2}(x\cos\theta + y\sin\theta). \tag{8}$$

The physical constants introduced to describe the Sun perturbation have to be in agreement with those of the EM model. Thus, the distance between the Sun and the Earth–Moon barycenter is $\rho = 3.8881\,10^2$, the mass of the Sun is $m_s = 3.2890\,10^5$, and its angular velocity with respect to the EM rotating frame is $\omega_S = -0.9251$. The Sun is located at $(\rho\cos\theta, \rho\sin\theta)$, and therefore its distance from P_3 is

$$r_s^2 = (x - \rho\cos\theta)^2 + (y - \rho\sin\theta)^2. \tag{9}$$

The *bicircular* four-body problem [11] is represented by the sixth-order system of Equations (7). The phase of the Sun, θ, is taken as problem state to let the system be autonomous. It is worth noting that this model is not coherent because all three primaries are assumed to move in circular orbits. Nevertheless, this model catches basic insights of the real four-body dynamics as the eccentricities of the Earth's and Moon's orbits are 0.016 and 0.054, respectively, and the Moon's orbit is inclined on the ecliptic by 5 deg.

3 Design Strategy

The transfers studied in this work are defined as follows. The spacecraft is assumed to be initially on a circular parking orbit around the Earth at a height $h = 200\,\text{km}$; an impulsive maneuver, Δv_{TLI}, carried out by the launch vehicle, places the spacecraft on a translunar trajectory; from this point on, the spacecraft can only rely on its low-thrust propulsion to reach a stable orbit around the Moon. This orbit has moderate eccentricity, e, and periapsis/apoapsis, r_p/r_a, prescribed by the mission requirements. The transfer terminates when the spacecraft is at the periapsis of the final orbit around the Moon. While both e and r_p/r_a are assumed to be given, the orientation, i.e., the argument of periapsis, ω, of the final orbit around the Moon is not fixed.

Low-energy, low-thrust transfers are achieved by optimizing, in a four-body scenario, a first guess derived by the coupled three-body problems approximation. Under this model, the transfer trajectory is conceived as made up by two distinct portions: the first, called Earth escape leg, is build in the SE model, whereas the second, called Moon low-thrust capture leg, is defined in the EM model.

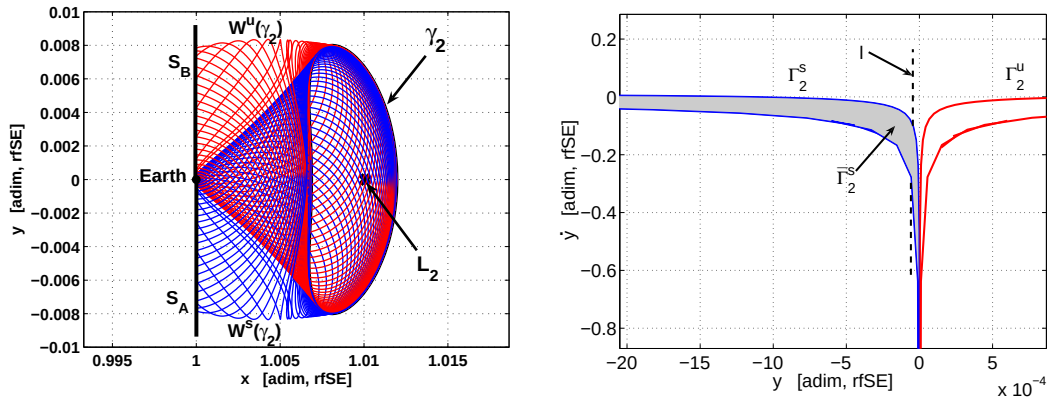

(a) $W^s(\gamma_2)$ and $W^u(\gamma_2)$. (b) Γ_2^s and Γ_2^u.

Fig. 1 Stable and unstable manifolds $W^s(\gamma_2)$, $W^u(\gamma_2)$ associated to the L_2 Lyapunov orbit γ_2, and their section curves Γ_2^s, Γ_2^u, respectively. In Figure 1(b), the set $\bar{\Gamma}_2^s$ (grey) is made up by the points of S_A that lie inside Γ_2^s, whereas the line l (dashed) is the locus of points being at 200 km altitude above the Earth's surface.

3.1 Earth Escape Leg

If a value of Jacobi constant in the SE model, C_{SE}, is suitably chosen, there exist a unique Lyapunov orbit about both L_1 and L_2, labeled γ_1 and γ_2, respectively. We consider energy values $C_{SE} \lesssim C_2$ such that both γ_1 and γ_2 exist, and the Hill's regions are opened at both L_1 and L_2. Without any loss of generality we construct the Earth escape leg considering the dynamics around L_2; using L_1 instead of L_2 is straightforward. The stable and unstable manifolds associated to γ_2, $W^s(\gamma_2)$ and $W^u(\gamma_2)$, are computed starting from the Lyapunov orbit until a certain surface of section is reached.

Since we aim at exploiting the structure of both $W^s(\gamma_2)$ and $W^u(\gamma_2)$, two surfaces of section are introduced to study their cuts at different stages. Section S_A, making an angle φ_A (clockwise) with the x-axis and passing through P_2, is considered to cut $W^s(\gamma_2)$, whereas section S_B, inclined by φ_B (counterclockwise) on the x-axis and passing through P_2, is assumed for $W^u(\gamma_2)$ (see Figure 1(a) where $\varphi_A = \varphi_B = \pi/2$). The corresponding section curves, Γ_2^s, Γ_2^u, represented on the $(r_2, \dot{r}_2)$-plane, are diffeomorphic to circles (in Figure 1(b), Γ_2^s, Γ_2^u are plotted on the $(y, \dot{y})$-plane as $r_2 = y$, $\dot{r}_2 = \dot{y}$ for $x = 1 - \mu$, $\varphi_A = \varphi_B = \pi/2$).

Both Poincaré sections represent two-dimensional maps for the flow of the RTBP. Indeed, any point on these sections uniquely defines an orbit. This property holds as both $\mathcal{J}(C_{SE})$ and $S_{A,B}$ lower the dimension of the phase space to two. By definition, points on Γ_2^s generate orbits that asymptotically approach γ_2 in forward time. Points inside Γ_2^s give rise to transit orbits that pass from the Earth region to the exterior region, whereas points outside Γ_2^s correspond to non-transit orbits (the manifolds act as separatrices for the states of motion [9, 10]).

Candidate trajectories for Earth–Moon transfers are non-transit orbits close to both $W^s(\gamma_2)$ and $W^u(\gamma_2)$. This property is wanted since the existence of $W^s(\gamma_2)$ and $W^u(\gamma_2)$ has to be exploited, although the transfer orbit does not exactly lie on any invariant subset. We label $\bar{\Gamma}_2^s$ as the set of points in the $(r_2, \dot{r}_2)$-plane that are enclosed by Γ_2^s (see Figure 1(b)). Points on $\bar{\Gamma}_2^s$ have to be avoided as they lead to either transit or asymptotic orbits. On the contrary, all the points that lie on

$$l = \{(r_2, \dot{r}_2) \in S_A,\ (r_2, \dot{r}_2) \notin \bar{\Gamma}_2^s | r_2 = h + R_E\}$$

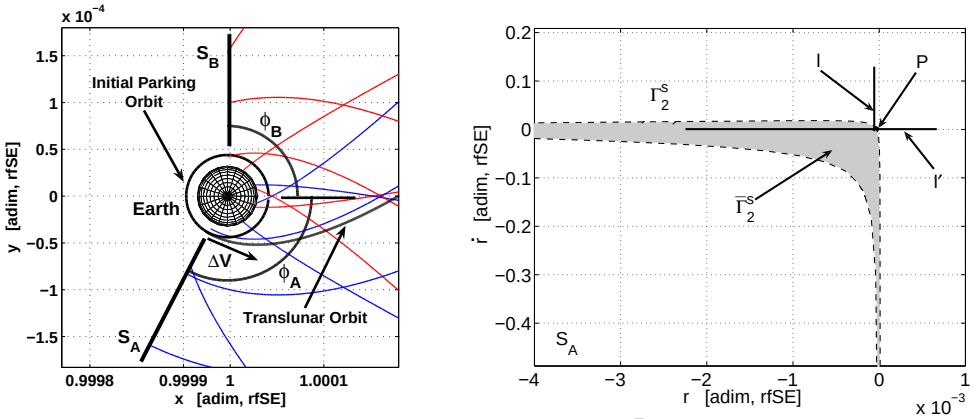

(a) Initial transfer condition.

(b) Γ_2^s, $\bar{\Gamma}_2^s$, l, l', and point $P = l \cap l'$.

Fig. 2 Earth escape trajectory performed with a tangential Δv_{TLI} maneuver and its associated section point P.

are translunar candidate orbits as they intersect the initial parking orbit (R_E is the radius of the Earth). This intersection occurs in the configuration space only as the initial parking orbit and the translunar trajectory have two different energy levels.

The pair $\{C_{SE}, \varphi_A\}$ uniquely defines the curve Γ_2^s on S_A: C_{SE} defines the orbit γ_2, whereas φ_A defines the surface of section S_A to cut the first intersection of $W^s(\gamma_2)$. Thus, $\{C_{SE}, \varphi_A\}$ are used to define the first guess Earth escape leg. In order to obtain efficient transfer trajectories, the lowest possible initial instantaneous maneuver, Δv_{TLI}, is searched. It is necessary to define its components: a first contribution to the Δv_{TLI} amount is related to the radial term Δv_r, while the second tangential contribution Δv_t is needed to fill the gap ΔC between the energy of the initial parking orbit, C_0, and C_{SE} (i.e., $\Delta C = C_0 - C_{SE}$). It is possible to show that $\Delta v(\Delta C, \varphi_A) = \Delta v_t(\Delta C) + \Delta v_r(\varphi_A)$, and it is even possible to lower Δv_r to zero by properly tuning φ_A. This approach leads to initial tangential maneuvers, i.e., the initial Δv_{TLI} is aligned with the velocity of the circular parking orbit around the Earth. The search is therefore restricted to the point $P \in S_A$ defined by $P = l \cap l'$, where l' is the set of points having zero radial velocity with respect to the Earth

$$l' = \{(r_2, \dot{r}_2) \in S_A,\ (r_2, \dot{r}_2) \notin \bar{\Gamma}_2^s | \dot{r}_2 = 0\}.$$

Point P does not exactly lie on the stable manifold, and can be found sufficiently close to $W^s(\gamma_2)$ by suitably tuning φ_A (see Figure 2). In practice, since at this stage we are building a first guess solution to be later optimized, orbits sufficiently close to P can also be considered. In particular, we consider points $P' \in S_A$ such that $|P' - P| \leq \epsilon$ as well, where ϵ is a certain prescribed distance.

A number of P' points can be generated by tuning the angle φ_A. These points, flown forward, generate orbits that are close to $W^s(\gamma_2)$ until the region about γ_2 is reached. From this point on, the orbits get close to $W^u(\gamma_2)$, and their intersection with S_B is studied. The set labeled $\mathcal{E}_{SE}$, $\mathcal{E}_{SE} \in S_B$, stands for the set of orbits close to $W^u(\gamma_2)$ whose pre-image $\mathcal{E}_{SE}^{-1}$, $\mathcal{E}_{SE}^{-1} \in S_A$, is made up by P' points. We take into account Earth escape trajectories defined on $\mathcal{E}_{SE}^{-1}$, $\mathcal{E}_{SE}$, as the latter intersects a special subset leading to low-thrust ballistic capture at the Moon (see Figure 3(b) where $\mathcal{E}_{SE}$ is reported).

It is worth noting that the parking orbit is defined at a lower energy level than orbits on $\mathcal{E}_{SE}^{-1}$, therefore the instantaneous velocity change Δv_{TLI} is required to place the translunar trajectory on $\mathcal{J}(C_{SE}) \cap \mathcal{E}_{SE}^{-1}$. In practice, this maneuver is provided by the launch vehicle once the spacecraft

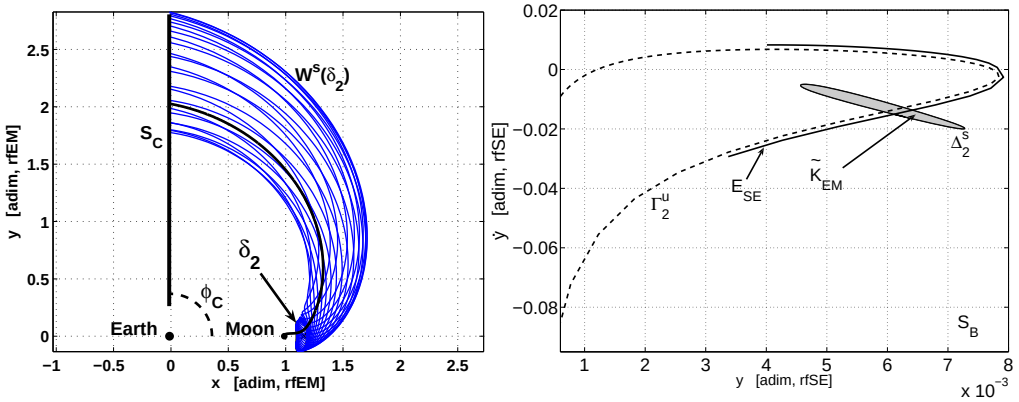

(a) $W^s(\delta_2)$. (b) Δ_s^2.

Fig. 3 Stable manifold $W^s(\delta_2)$ and its section curve Δ_2^s. The latter is used to define the set of orbits that lead to Moon capture $\mathcal{K}_{EM}$ (this set is labeled $\tilde{\mathcal{K}}_{EM}$, in gray in Figure 3(b), when reported on S_B).

is on the Earth parking orbit. A mission profile including this parking orbit is in fact consistent with major architecture requirements [12].

The design of the SE phase is reduced in this way to the determination of just the two sets $\mathcal{E}_{SE}^{-1}$, $\mathcal{E}_{SE}$, and to the computation of Δv_{TLI}. This first phase of the transfer is constructed using either equations (1) or equations (6) with $T = 0$. The SE trajectory does not make use of low-thrust propulsion, and the phase space structure of the ballistic RTBP is exploited.

3.2 Moon Ballistic Capture Leg

By fixing a suitable value of the Jacobi constant in the EM model, C_{EM}, a unique Lyapunov orbit about both L_1 and L_2, named δ_1 and δ_2, respectively, can be defined. Restricting the energy to $C_{EM} \lesssim C_2$, both δ_1 and δ_2 exist, and the Hill's regions are opened at both L_1 and L_2. In order to reach the final orbit about the Moon from the exterior, a capture via L_2 is considered (see Figure 3(a)). This means that we construct the Moon ballistic capture leg by exploiting the dynamics around L_2. The stable manifold associated to δ_2, $W^s(\delta_2)$, is computed starting from δ_2 and integrating backward until a certain surface of section is reached. Section S_C, making an angle φ_C (counterclockwise) with the x-axis and passing through P_1, is considered to cut $W^s(\delta_2)$ ($\varphi_C = \pi/2$ in Figure 3(a)). The corresponding section curve, Δ_2^s represented on the $(r_1, \dot{r}_1)$-plane, is diffeomorphic to a circle. We can now define $\mathcal{K}_{EM} = \bar{\Delta}_2^s$, where $\bar{\Delta}_2^s \in S_C$ is the set of points inside Δ_2^s, as the set that leads to Moon capture.

The set $\mathcal{K}_{EM}$ is defined on section S_C in the EM model. However, it is possible to represent $\mathcal{K}_{EM}$ on S_B defined in the SE model through the transformation $\tilde{\mathcal{K}}_{EM} = \mathcal{M}(\mathcal{K}_{EM})$. The operator $\mathcal{M}$ maps states on S_C (EM model) to states on S_B (SE model), provided the two angles φ_C, φ_B. This transformation is basically made up by a rotation and a rescaling of the variables in proper units (see Figure 3(b) where $\tilde{\mathcal{K}}_{EM}$ is reported).

Considering the sole section S_B, it is possible to define the *ballistic* low energy Earth–Moon transfers as the orbits belonging to the set $\mathcal{E}_{SE} \cap \tilde{\mathcal{K}}_{EM}$. The sets $\mathcal{E}_{SE}$ and $\tilde{\mathcal{K}}_{EM}$ are characterized by different values of the Jacobi constant, C_{SE} and C_{EM}, respectively. In addition, any point in $\tilde{\mathcal{K}}_{EM}$ has a different value of Jacobi constant as $\mathcal{M}$ is not energy preserving. Thus, in order to join together orbits on $\mathcal{E}_{SE}$ and orbits on $\tilde{\mathcal{K}}_{EM}$, it is necessary to perform an impulsive maneuver at the patching point.

This approach is the one known in literature to design Earth–Moon low energy transfers with impulsive maneuvers [3]. Indeed, another impulsive maneuver, beside the one performed at the patching point, is necessary upon Moon arrival to place the spacecraft into a stable orbit around the Moon. This approach is based on either equations (1) or equations (6) with $T = 0$, and allows us to define low energy transfers like those described in [1–3]. Nevertheless, this method is not suitable to design low-energy, low-thrust Earth–Moon transfers as impulsive maneuvers cannot be provided by low-thrust systems. A modification is therefore necessary. In particular, the definition of a low-thrust capture set, analogous to $\mathcal{K}_{EM}$, has to be given in order to construct low-energy, low-thrust transfers in a totally analogous fashion.

3.3 Moon Low-Thrust Capture Leg

Without any loss of generality, let us assume a final orbit around the Moon with eccentricity $e = 0.65$; this is associated, approximately, to an elliptic orbit with pericenter and apocenter altitudes $h_p = 1000\,\text{km}$ and $h_a = 10000\,\text{km}$, respectively. The final condition of the transfer is set to $\mathbf{y}_p$, which is the vector made up by the spacecraft state (position and velocity) at the pericenter of the arrival lunar orbit.

We aim to achieve the capture by application of a continuous low-thrust control law. When the maximum thrust T_{max} is applied tangentially, the state $\mathbf{y}(t)$ of a generic point along the propelled leg can be defined by backward flowing system (6) starting from the pericenter. Let $\phi_{\mathbf{T}(t)}(\mathbf{x}_0, t_0; t)$ be the flow of system (6) starting from $(\mathbf{x}_0, t_0)$ and considering the thrust $\mathbf{T}(t)$. With this notation, it is possible to define the generic point of the low-thrust capture leg through

$$\mathbf{y}(t) = \phi_{\bar{\mathbf{T}}}(\mathbf{y}_p, t_f; t), \tag{10}$$

where t_f is the final time, $t \leq t_f$, and $\bar{\mathbf{T}} = T_{max}\mathbf{v}/\|\mathbf{v}\|$, $\mathbf{v} = (\dot{x}, \dot{y})$. The point $\mathbf{y}(t)$ is defined for $t \in [\tau, t_f]$, where τ is the time starting from which the engine is on duty at the maximum thrust level. If ω indicates the argument of pericenter of the elliptic orbit around the Moon, the couple $\{\tau, \omega\}$ uniquely specifies the point $\mathbf{y}(\tau)$ in the phase space. Thus, $\{\tau, \omega\}$ can be suitably tuned for the construction of the first guess low-thrust capture solution (see Figure 4(a)).

As for the ballistic case discussed previously, we can define on section S_C the *low-thrust capture* set, $\mathcal{L}_{EM} = \{\gamma_{\bar{\mathbf{T}}}(\omega) \cap S_C, \forall \omega \in [0, 2\pi]\}$, where $\gamma_{\bar{\mathbf{T}}}(\omega) = \{\phi_{\bar{\mathbf{T}}}(\mathbf{y}_p(\omega), t_f; \tau) | \forall \tau < t_f\}$ is the low-thrust orbit flown backward starting from the periapsis. It is possible to represent the set $\mathcal{L}_{EM}$ on section S_B by application of the previously defined operator $\mathcal{M}$, i.e., $\tilde{\mathcal{L}}_{EM} = \mathcal{M}(\mathcal{L}_{EM})$ (see Figure 4(b)). As for $\tilde{\mathcal{K}}_{EM}$ in section 3.2, the set $\tilde{\mathcal{L}}_{EM}$ is not necessary made up by points having the same value of Jacobi constant. Nevertheless, by varying $\{\tau, \omega\}$, the set $\tilde{\mathcal{L}}_{EM}$ can be forced to have the energy level C_{SE}, that is the energy level of the Earth escape orbits.

Thanks to the definition of $\tilde{\mathcal{L}}_{EM}$, the low-energy, low-thrust transfers can be defined using the same concept behind the ballistic Earth–Moon transfers. Indeed, $\mathcal{E}_{SE}$ is the set containing Earth escape trajectory, whereas $\tilde{\mathcal{L}}_{EM}$ is made up by low-thrust capture orbits. Thus, when these two sets are reported on the same surface of section, S_B in this case, the low-energy, low-thrust orbits are simply defined as those orbits generated by $\mathcal{E}_{SE} \cap \tilde{\mathcal{L}}_{EM}$. This is a significant departure from classic Earth–Moon low-thrust transfers as in this case the structure of the phase space of the two RTBP is exploited. Moreover, since $\tilde{\mathcal{L}}_{EM}$ is forced to lie on $\mathcal{J}(C_{SE})$, no velocity discontinuity is achieved at the patching point.

In summary, the first guess solution is made up by pieces defined in two RTBP. The Earth escape leg, derived in the SE model, considers system of equations (1), and therefore it makes use of the Sun–Earth dynamics in a ballistic fashion (i.e., no low-thrust is considered in this first leg). The Moon low-thrust capture leg is derived by equations (6) employing a tangential thrust policy. These two pieces are patched together to form a first guess solution. This is the essence of the coupled restricted three-body problems approximation.

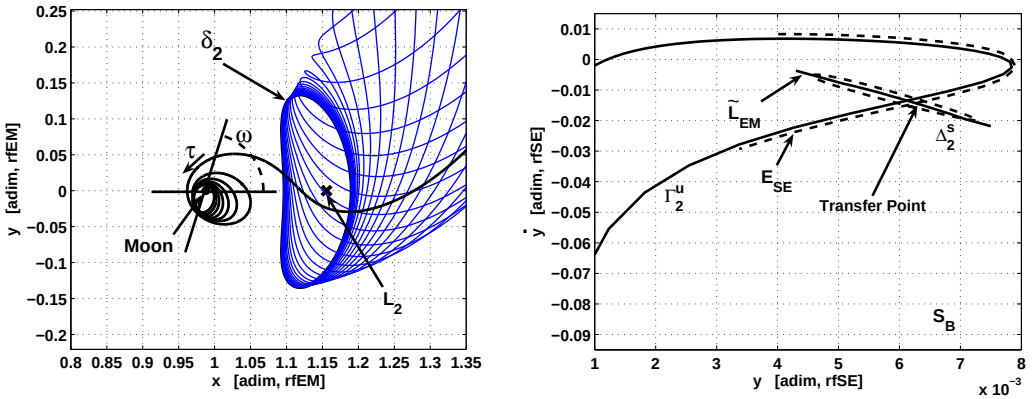

(a) Low-thrust capture trajectory. (b) $\tilde{\mathcal{L}}_{EM}$ and $\mathcal{E}_{SE}$ sets.

Fig. 4 The first guess low-thrust capture solution as the point $\mathcal{E}_{SE} \cap \tilde{\mathcal{L}}_{EM}$ on S_B.

4 Transfer Optimization

Once feasible and efficient first guess trajectories are achieved with the low-thrust version of the patched restricted three-body problems approximation, an optimal control problem is stated in the complete four-body dynamics. Taking into account the low-thrust propulsion and the gravitational attractions of the Sun, the Earth, and the Moon (through the controlled bicircular four-body problem given in Section 2.2), it is possible to further improve the first guess solutions found. In particular, we aim at finding, according to the standard optimal control theory [13], the guidance law $\mathbf{T}(t)$, $t \in [t_0, t_f]$, that minimizes the performance index

$$J = m_p, \tag{11}$$

where $m_p = m_0 - m(t_f)$ stands for the propellant mass needed to carry out the transfer, m_0 is the wet mass placed in the translunar orbit, and $m(t_f)$ is the spacecraft mass depending upon the optimal control policy $\mathbf{T}(t)$ through the last of equations (7). In order to make the whole optimization robust, each first guess is first processed to minimize

$$J = \frac{1}{2} \int_{t_0}^{t_f} \mathbf{u}^T \mathbf{u} \, \mathrm{d}t, \tag{12}$$

with $\mathbf{u}(t) = \mathbf{T}(t)/m(t)$, and the resulting solution is later used to minimize objective function (11). Numerical experiments have shown that performing an intermediate step with objective function (12) better enforces the respect of boundary conditions and path constraints.

The initial boundary condition defines the tangential departure from a circular parking orbit around the Earth; the final boundary condition states the arrival at the pericenter of the final orbit about the Moon. Eccentricity and pericenter altitude of this orbit are prescribed my mission requirements. The path constraint is used to model the saturation of the low-thrust engine. Thus, the inequality $T(t) \leq T_{max}$, $t \in [t_0, t_f]$, is imposed along the whole transfer with $T_{max} = 0.5\,\mathrm{N}$.

The optimal control has been solved using a direct approach. This approach, although sub-optimal, generally shows robustness and versatility, and does not require explicit derivation of the necessary conditions of optimality. Moreover, direct approaches offer higher computational efficiency and are less sensitive to variation of the first guess solutions [14]. In this paper we have implemented a direct multiple shooting method, in agreement with the terminology introduced in [14]. With this strategy the RFBP dynamics is forward integrated within a number of sub-intervals (in which $[t_0, t_f]$ is split) and the continuity of position and velocity is imposed at

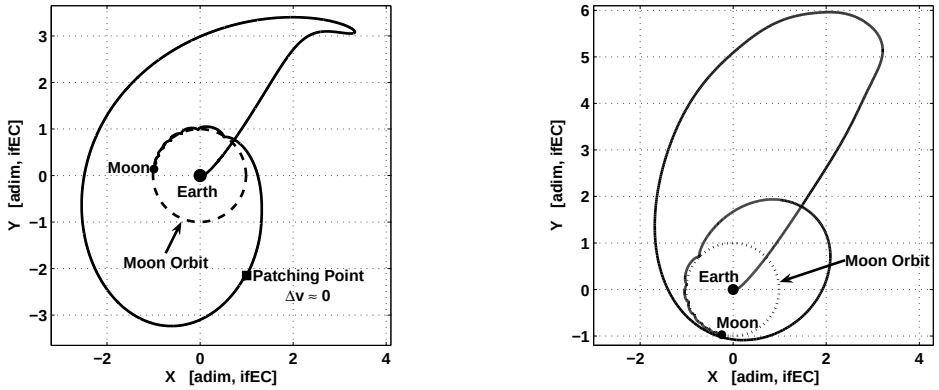

(a) First guess solution. (b) Optimized trajectory.

Fig. 5 A first guess solution achieved by the low-thrust restricted three-body problem approximation and the corresponding optimal trajectory.

their ends [15]. The control law $\mathbf{T}(t)$ is described within each sub-interval by means of cubic spline functions. The algorithm computes the value of the control at mesh points, respecting both boundary and path constraints, and minimizing the performance index.

Dynamics (7) are highly nonlinear and, in general, lead to chaotic orbits. In order to find accurate optimal solutions without excessively increasing the computational burden, an adaptive nonuniform time grid has been implemented. Thus, when the trajectory is close to either the Earth or the Moon the grid is automatically refined, whereas in the intermediate phase, where a weak vector field governs the motion of the spacecraft, a coarse grid is used. The optimal solution found is assessed a posteriori by forward integrating the optimal initial condition and by cubic interpolation of the discrete optimal control solution. In Figure 5 we have reported a typical first guess solution (Figure 5(a)) and the associated optimal solution defined under the four-body dynamics (Figure 5(b)). It can be seen that the optimization converges to a final solution that is quite different from the initial guess. This indicates that the implemented numerical scheme is able to explore wide areas of the solutions space, though the optimal control problem is solved via local methods [14].

5 Low-Energy, Low-Thrust Transfers

In this section we present the low-energy, low-thrust (LELT) solutions achieved with the method described so far. Table 1 summarizes three sample solutions that are compared to some reference transfers found in literature [1, 12, 16, 17]. It is worth pointing out that the reference solutions have been achieved with impulsive maneuvers, therefore their comparison to the LELT solutions should be made in terms of propellant mass ratio. In Table 1, the term Δv_{TLI} stands for the cost of the translunar injection maneuver, assumed to be performed by the launch vehicle once the spacecraft is on a 200 km circular parking orbit about the Earth. The propellant mass fraction, m_p/m_0, is computed assuming $m_0 = 1000\,\mathrm{kg}$. For the LELT solutions, the specific impulse $I_{sp}^{LT} = 3000\,\mathrm{s}$ has been used to integrate the last of equations (7). For the sake of consistency, the propellant mass fraction of the reference, high-thrust solutions has been computed through the rocket equation

$$\frac{m_p}{m_0} = 1 - \exp\left(-\frac{\sum_i \Delta v_i}{I_{sp}^{HT} g_0}\right) \tag{13}$$

Type	Δv_{TLI} [m/s]	$\sum_i \Delta v_i$ [m/s]	e [–]	h_p [km]	m_p/m_0 [–]	Δt [days]
LELT #1	3195	—	0.65	1000	0.031	236
LELT #2	3207	—	0.65	1000	0.032	228
LELT #3	3203	—	0	100	0.061	271
WSB [1]	3161	677	0	100	0.205	90-120
BP [1]	3232	721	0	100	0.217	∞
HO [1]	3143	848	0	100	0.253	4-5
BE [1]	3161	987	0	100	0.285	55-90
L1 [16]	3265	629	0	100	0.192	255
MIN [17]	3099	622	0	100	0.190	—

Table 1 Comparison between the low-energy, low-thrust (LELT) solutions designed and a set of impulsive reference solutions found in literature. (WSB: weak stability boundary; BP: bi-parabolic; HO: Hohmann; BE: bi-elliptic; L1: via L_1 transit orbits; MIN: minimum theoretical). Reference solutions are relative to a 167 km circular parking orbit about the Earth.

where $I_{sp}^{HT} = 300\,\mathrm{s}$, and Δv_i are the magnitudes of the impulsive maneuvers necessary to carry out the transfer except Δv_{TLI} (e.g., for an Hohmann transfer, Δv_i is the magnitude of the sole second burn necessary to place the spacecraft into the final orbit around the Moon; for a WSB transfer, this term has to take into account the eventual mid-course maneuver as well as the final maneuver needed to place the spacecraft into the final orbit about the Moon; similar arguments apply also to the bi-elliptic and bi-parabolic transfers. The minimum theoretical cost is computed via energetic considerations, and no solutions corresponding to such solution exist.). Three more columns are reported in Table 1: e and h_p are the eccentricity and the periapsis altitude of the final orbit about the Moon, respectively, whereas Δt is the flight time.

The first two rows are relative to low-energy, low-thrust transfers leading to an elliptic orbit around the Moon with $e = 0.65$ and $h_p = 1000\,\mathrm{km}$. The TLI impulse for these two solutions is slightly higher than Δv_{TLI} of both Hohmann and WSB transfers. However, the propellant mass necessary for the rest of the transfer is significantly lower than that associated to all reference cases. This is due to the low-thrust specific impulse, I_{sp}^{LT}, that is one order of magnitude greater than I_{sp}^{HT}, assumed in equation (13) to evaluate the propellant mass fraction of the reference solutions. Moreover, the final orbit about the Moon in these two cases has an higher semi-major axis than that of the reference solutions. Another relevant feature of the LELT solutions presented is the transfer time. In the stated approach the propellant mass has been minimized without any constraint on the time of flight. This has led to very efficient solutions from the propellant mass ratio point of view that require a longer transfer time compared to that of the reference solutions.

Figure 6 shows the solution LELT #1. In details, the transfer orbit presented in the Earth-centered frame (Figure 6(a)) shows a capture mechanism which takes advantage of a 3:1 resonance with the Moon. Moreover, the furthest point of the trajectory from the Earth is approximately six times the Earth–Moon distance. Across this region, even if not present in the first guess solution, a very low-thrust arc is attained in the optimization step (from T_{on} to T_{off} in Figures 6(a)).

In solution LELT #3, the final orbit about the Moon overlaps with that assumed in the reference solutions. Thus, a coherent comparison can be performed in this case. Although the magnitude of Δv_{TLI} is slightly higher, the LELT method has been able to deliver a solution outperforming all the reference ones in terms of propellant mass fraction by one order of magnitude.

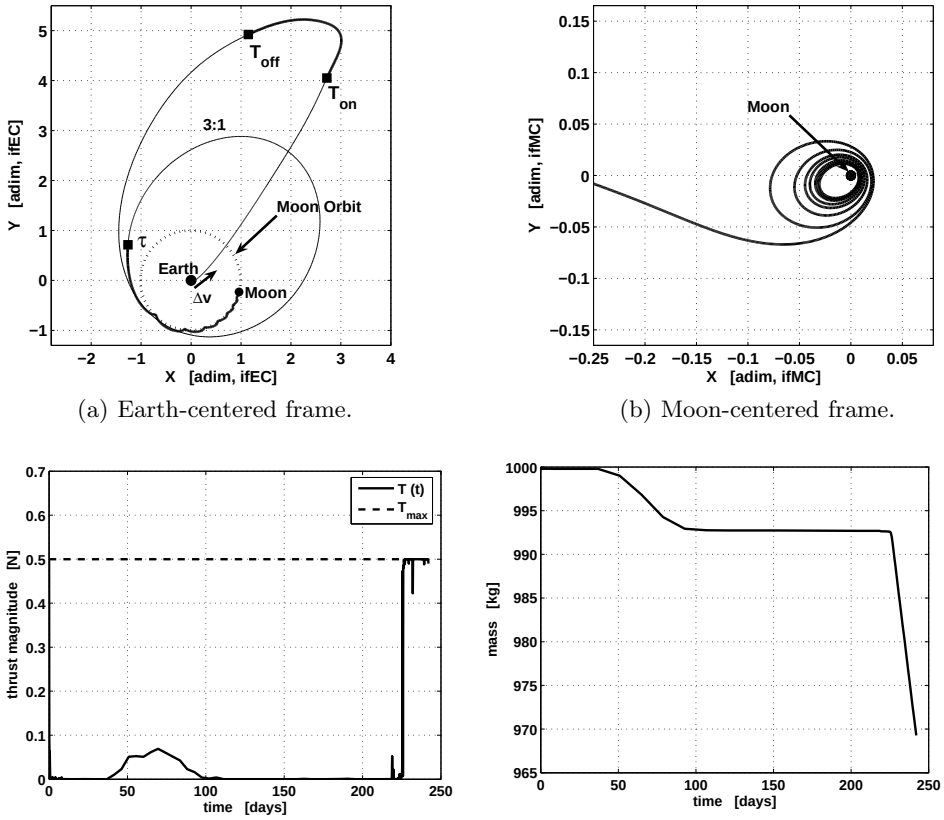

(a) Earth-centered frame.

(b) Moon-centered frame.

(c) Thrust profile.

(d) Mass consumption.

Fig. 6 LELT solution #1 in Table 1. The solution is presented in terms of transfer trajectory, thrust profile, and mass consumption. It is important to note that, since in the optimization process the low-thrust is not constrained to act in the capture leg only, but rather it is a free parameter that has to be found along the whole trajectory, a thrust arc is achieved when the spacecraft is far from the Earth at about six Earth–Moon distances. This indicates that in such region it is possible to suitably tune the spacecraft state with little expenses of propellant. In the subsequent coast arc (at constant mass) a Moon gravity assist places the spacecraft into a 3:1 resonant orbit with the Moon which leads to the low-thrust Moon capture.

6 Conclusions

A systematic method for the design of low-energy, low-thrust transfers has been described in this paper. A first guess solution with no velocity discontinuity at the patching point is achieved with the low-thrust version of the coupled three-body problems approximation. In this framework the low-thrust Moon leading set is defined and the whole design is reduced to the search of a single point on a suitable surface of section. The first guess so derived is later optimized in the controlled four-body dynamics using a direct multiple shooting strategy. We have shown that the formulated method delivers very efficient solution requiring much less propellant than the standard impulsive low energy transfers.

Acknowledgments

The authors would like to acknowledge Dr. Ed Belbruno for the useful discussions which paved the way to the work described in this paper.

References

1. E. Belbruno and J. Miller, Sun-Perturbated Earth-to-Moon Transfers with Ballistic Capture, Journal of Guidance, Control and Dynamics, 16, 770–775 (1993)
2. E. Belbruno, The Dynamical Mechanism of Ballistic Lunar Capture Transfers in the Four-Body Problem from the Perspective of Invariant Manifolds and Hill's Regions, Technical Report, Centre de Recerca Matematica, Barcelona, Spain (1994)
3. W. Koon, M. Lo, J. Marsden, and S. Ross, Low Energy Transfer to the Moon, Celestial Mechanics and Dynamical Astronomy, 81, 63–73 (2001)
4. E. Belbruno, Lunar Capture Orbits, a Method of Constructing Earth–Moon Trajectories and the Lunar GAS Mission, AIAA Paper no. 97-1054, Proceedings of AIAA/DGLR/JSASS International Electric Propulsion Conference (1987)
5. J. Schoenmaekers, D. Horas, and J. A. Pulido, SMART-1: With Solar Electric Propulsion to the Moon, Proceedings of the 16th International Symposium on Space Flight Dynamics (2001)
6. M. Dellnitz, O. Junge, M. Post, and B. Thiere, On Target for Venus – Set Oriented Computation of Energy Efficient Low Thrust Trajectories, Celestial Mechanics and Dynamical Astronomy, 95, 357–370 (2006)
7. G. Mingotti, F. Topputo, and F. Bernelli-Zazzera, Combined Optimal Low-Thrust and Stable-Manifold Trajectories to the Earth–Moon Halo Orbits, American Institute of Physics Conference Proceedings, 886, 100–110 (2007)
8. V. Szebehely, Theory of Orbits: The Restricted Problem of Three Bodies, Academic Press Inc., New York (1967)
9. C. Conley, Low Energy Transit Orbits in the Restricted Three-Body Problem, SIAM Journal of Applied Mathematics, 16, 732–746 (1968)
10. J. Llibre, R. Martinez, and C. Simó, Transversality of the Invariant Manifolds associated to the Lyapunov Family of Periodic Orbits near L_2 in the Restricted Three-Body Problem, Journal of Differential Equations, 58, 104–156 (1985)
11. C. Simó, G. Gómez, À Jorba, and J. Masdemont, The Bicircular Model near the Triangular Libration Points of the RTBP, From Newton to Chaos, Plenum Press, New York, 343–370 (1995)
12. E. Perozzi and A. Di Salvo, Novel Spaceways for Reaching the Moon: an Assessment for Exploration, Celestial Mechanics and Dynamical Astronomy, 102, 207–218 (2008)
13. A. Bryson and Y. Ho, Applied Optimal Control, John Wiley & Sons, New York (1975)
14. J. Betts, Survey of Numerical Methods for Trajectory Optimization, Journal of Guidance, Control, and Dynamics, 21, 193–207 (1998)
15. P. Enright and B. Conway, Discrete Approximations to Optimal Trajectories using Direct Transcription and Nonlinear Programming, Journal of Guidance, Control, and Dynamics, 15, 994–1002 (1992)
16. F. Topputo, M. Vasile, and F. Bernelli-Zazzera, Earth-to-Moon Low Energy Transfers Targeting L_1 Hyperbolic Transit Orbits, Annals of the New York Academy of Sciences, 1065, 55–76 (2005)
17. T. Sweetser, An Estimate of the Global Minimum Δv needed for Earth–Moon Transfer, Advances in the Astronautical Sciences Series, 75, 111–120 (1991)